Inorg. Chem. **2008**, *47*, 5736−5745

Synthesis, Structures, and Magnetic Properties of Face-Sharing Heterodinuclear Ni(II)−Ln(III) (Ln = Eu, Gd, Tb, Dy) Complexes

Tomoka Yamaguchi,[†] Yukinari Sunatsuki,[†] Hiroyuki Ishida,[†] Masaaki Kojima,[*,†] Haruo Akashi,[‡] Nazzareno Re,[*,§] Naohide Matsumoto,[||] Andrzej Pochaba,[⊥] and Jerzy Mroziński[⊥]

Department of Chemistry, Faculty of Science, Okayama University, Tsushima-naka 3-1-1, Okayama 700-8530, Japan, Research Institute of Natural Sciences, Okayama University of Science, Ridai-cho, Okayama 700-0005, Japan, Facolta di Farmacià, Universita degli Studi "G. D'Annunzio", I-66100 Chieti, Italy, Department of Chemistry, Faculty of Science, Kumamoto University, Kumamoto 860-8555, Japan, and Faculty of Chemistry, University of Wrocław, 14 F. Joliot-Curie, 50-383 Wrocław, Poland

Received January 12, 2008

Heterodinuclear $[(Ni^{II}L)Ln^{III}(hfac)_2(EtOH)]$ (H_3L = 1,1,1-tris[(salicylideneamino)methyl]ethane; Ln = Eu, Gd, Tb, and Dy; hfac = hexafluoroacetylacetonate) complexes (**1**·**Ln**) were prepared by treating $[Ni(H_{1.5}L)]Cl_{0.5}$ (**1**) with $[Ln(hfac)_3(H_2O)_2]$ and triethylamine in ethanol (1:1:1). All **1**·**Ln** complexes (**1**·**Eu**, **1**·**Gd**, **1**·**Tb**, and **1**·**Dy**) crystallized in the triclinic space group $P\bar{1}$ (No. 2) with $Z = 2$ with very similar structures. Each complex is a face-sharing dinuclear molecule. The Ni^{II} ion is coordinated by the L^{3-} ligand in a N_3O_3 coordination sphere, and the three phenolate oxygen atoms coordinate to an Ln^{III} ion as bridging atoms. The Ln^{III} ion is eight-coordinate, with four oxygen atoms of two $hfac^-$'s, three phenolate oxygen atoms of L^{3-}, and one ethanol oxygen atom coordinated. Temperature-dependent magnetic susceptibility and field-dependent magnetization measurements showed a ferromagnetic interaction between Ni^{II} and Gd^{III} in **1**·**Gd**. The Ni^{II}−Ln^{III} magnetic interactions in **1**·**Eu**, **1**·**Tb**, and **1**·**Dy** were evaluated by comparing their magnetic susceptibilities with those of the isostructural Zn^{II}−Ln^{III} complexes, $[(ZnL)Ln(hfac)_2(EtOH)]$ (**2**·**Ln**) containing a diamagnetic Zn^{II} ion. A ferromagnetic interaction was indicated in **1**·**Tb** and **1**·**Dy**, while the interaction between Ni^{II} and Eu^{III} was negligible in **1**·**Eu**. The magnetic behaviors of **1**·**Dy** and **2**·**Dy** were analyzed theoretically to give insight into the sublevel structures of the Dy^{III} ion and its coupling with Ni^{II}. Frequency dependence in the ac susceptibility signals was observed in **1**·**Dy**.

Introduction

Single-molecule magnets (SMMs) have attracted special attention, because they provide unique opportunities for the investigation of such behaviors as magnetic hysteresis and quantum tunneling of the magnetization resulting from slow magnetic relaxation.[1] They can be applied to magnetic information storage devices on the molecular scale and to quantum-based computers.[2] Studies on SMMs based on metal complexes have been carried out mostly on 3d-metal cluster systems such as Mn_{12}[1a,b] and Fe_8.[1g] These SMMs have a high-spin ground-state and a large easy axis magnetic anisotropy, with a negative zero field splitting (ZFS) parameter, D. The past decade has seen a burst of activity in SMM research based on these 3d-metal cluster systems, and the fine details have become better understood. However, the blocking temperatures, T_B, of the SMMs reported so far are still quite low, and new molecular designs are needed.

* Corresponding author fax: +81-86-251-7842; e-mail: kojima@cc.okayama-u.ac.jp.
[†] Okayama University.
[‡] Okayama University of Science.
[§] Universita degli Studi "G. D'Annunzio".
[||] Kumamoto University.
[⊥] University of Wrocław.

(1) (a) Sessoli, R.; Tsai, H.; Schake, A. R.; Wang, S.; Vincent, J. B.; Folting, K.; Gatteschi, D.; Christou, G.; Hendrickson, D. N. *J. Am. Chem. Soc.* **1993**, *115*, 1804–1816. (b) Sessoli, R.; Gatteschi, D.; Caneschi, A.; Novak, M. A. *Nature* **1993**, *365*, 141–143. (c) Gatteschi, D.; Caneschi, A.; Pardi, L.; Sessoli, R. *Science* **1994**, *265*, 1054–1058. (d) Thomas, L.; Lionti, F.; Ballou, R.; Gatteschi, D.; Sessoli, R. *Nature* **1996**, *383*, 145–147. (e) Friedman, J. R.; Sarachik, M. P.; Tejada, J.; Ziolo, R. *Phys. Rev. Lett.* **1996**, *76*, 3830–3833. (f) Aromi, G.; Barbara, B.; Brechin, E. K.; Caneschi, A. *Single Molecule Magnets and Related Phenomena*; Springer: New York, 2006. (g) Barra, A. L.; Debrunner, P.; Gatteschi, D.; Schultz, Ch. E.; Sessoli, R. *Europhys. Lett.* **1996**, *35*, 133–138.

10.1021/ic8000575 CCC: $40.75
Published on Web 05/31/2008

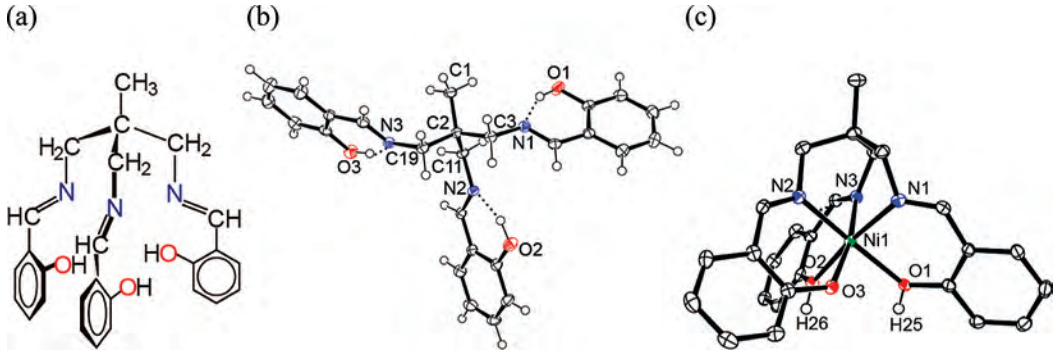

Figure 1. Structures of the H_3L ligand and $[Ni(H_{1.5}L)]Cl_{0.5}\cdot MeOH$ (**1**). (a) The structural formula of the tripodal H_3L ligand. (b) ORTEP drawing of the H_3L ligand with atom numbering scheme showing the 50% probability ellipsoids. (c) ORTEP drawing of the complex cation of $[Ni(H_{1.5}L)]Cl_{0.5}\cdot MeOH$ (**1**). The hydrogen atoms on carbon atoms are omitted for clarity.

In order to create different families of compounds showing slow magnetization relaxation, several research groups are starting to branch out into such fields as SMMs based on 3d−5d[3] and 3d−4f complexes[4] and single-chain magnets.[5]

We paid attention to the work of Ishikawa's group. They reported that Tb^{III}, Dy^{III}, and Ho^{III} phthalocyanines exhibit SMM behavior, showing that even a mononuclear 4f molecule can be a SMM.[6] Lanthanide (Ln) metal ions have a large ground-state spin and a strong easy axis magnetic anisotropy, and the magnetic interactions of many 3d−4f complexes have been reported to be ferromagnetic.[4a,b] All of these properties are favorable for 3d−4f complexes to behave as SMMs. Polynuclear 3d−4f complexes will meet the requirement to be identified as SMMs by a smaller number of metal ions than the 3d-transition metal clusters. Therefore, 3d−4f complexes are strong candidates for SMMs. Actually, a new class of 3d−4f SMMs including Cu_2Tb_2,[4a,b,o] Cu_2Dy_2,[4a–c,o] Mn_6Dy_6,[4d] $Mn_{11}Dy_4$,[4e] Mn_2Dy_2,[4f] $CuDy_2$,[4g] FeDy,[4h] $CuTb_4$,[4i] $NiDy_2$,[4j] Cu_6Dy_3,[4k] $FeDy_2$,[4l] CuTb,[4m] and $Mn_{11}Gd_2$[4n] has been reported, and the 3d−4f complex approach is a promising pathway to SMMs. However, there are still insufficient studies of 3d−4f complexes examining the construction of SMMs, due mainly to synthetic difficulties. In order to create a 3d−4f SMM system, it is necessary to develop synthetic procedures; control of the nuclearity of the complex is especially important. Recently, we have prepared di-, tri-, and tetranuclear Ni^{II}−Gd^{III} complexes by the use of the "complexes-as-ligands" strategy, and we could control the nuclearity of the complexes by the selection of the additional ligand on the Gd^{III} ion.[7] This paper reports the structures and magnetic properties of the dinuclear $[(Ni^{II}L)Ln^{III}(hfac)_2(EtOH)]$ (Ln = Eu, Gd, Tb, Dy, hfac = hexafluoroacetylacetonate, H_3L = 1,1,1-tris[(salicylideneamino)methyl]ethane; Figure 1) complexes.

Results and Discussion

Synthesis, Characterization, and Structures of H_3L and Dinuclear $Ni^{II}Ln^{III}$ (1·Ln) and $Zn^{II}Ln^{III}$ (2·Ln) Complexes. In a previous paper,[8] we reported that the reaction of $NiCl_2\cdot 6H_2O$ with the tripodal ligand H_3L afforded two types of complexes, mononuclear $[Ni(H_{1.5}L)]Cl_{0.5}$ and trinuclear $[Ni_3L_2]$. When $NiCl_2\cdot 6H_2O$ and H_3L were allowed to react in a 1:1 molar ratio without the addition of a base, the mononuclear complex was exclusively obtained. The complex has a dimeric structure: two mononuclear units are linked by O(phenol)−H···O(phenolate) hydrogen bonds. When Ni^{II} was allowed to react with H_3L in the presence of triethylamine (3:2:6), the linear trinuclear $[Ni_3L_2]$ formed. Heterotrinuclear complexes $[M(NiL)_2]$ (M = Mn, Co) were prepared by the reaction of $[Ni(H_{1.5}L)]Cl_{0.5}$ with M^{II} (2:1) in the presence of a base.[8,9] In refs 8 and 9, the mononuclear complex has been reported to be [Ni(HL)]. However, a detailed structure analysis revealed that it is actually

(2) (a) Wernsdorfer, W.; Aliaga-Alcade, N.; Hendrickson, D. N.; Christou, G. *Nature* **2002**, *416*, 406–409. (b) Leuenberger, M. N.; Loss, D. *Nature* **2001**, *410*, 789–793.

(3) Shelter, E. J.; Prosvirin, A. V.; Dunbar, K. R. *J. Am. Chem. Soc.* **2004**, *126*, 15004–15005.

(4) (a) Osa, S.; Kido, T.; Matsumoto, N.; Re, N.; Pochaba, A.; Mroziński, J. *J. Am. Chem. Soc.* **2004**, *126*, 420–421. (b) Hamamatsu, T.; Yabe, K.; Towatari, M.; Osa, S.; Matsumoto, N.; Re, N.; Pochaba, A.; Mrozinlski, J.; Gallani, J.-L.; Barla, A.; Imperia, P.; Paulsen, C.; Kappler, J.-P. *Inorg. Chem.* **2007**, *46*, 4458–4468. (c) Costes, J.-P.; Auchel, M.; Dahan, F.; Peyrou, V.; Shova, S.; Wernsdorfer, W. *Inorg. Chem.* **2006**, *45*, 1924–1934. (d) Zaleski, C. M.; Depperman, E. C.; Kampf, J. W.; Kirk, M. L.; Pecoraro, L. *Angew. Chem., Int. Ed.* **2004**, *43*, 3912–3914. (e) Mishra, A.; Wersdorfer, W.; Abboud, K. A.; Christou, G. *J. Am. Chem. Soc.* **2004**, *126*, 15648–15649. (f) Mishra, A.; Wersdorfer, W.; Parsons, S.; Christou, G.; Brechin, E. K. *Chem. Commun.* **2005**, 2086–2088. (g) Mori, F.; Nyui, T.; Ishida, T.; Nogami, T.; Choi, K.-Y.; Nojiri, H. *J. Am. Chem. Soc.* **2006**, *128*, 1440–1441. (h) Ferbinteanu, M.; Kajiwara, T.; Choi, K.-Y.; Nojiri, H.; Nakamoto, A.; Kojima, N.; Cimpoesu, F.; Fujimura, Y.; Takaishi, S.; Yamashita, M. *J. Am. Chem. Soc.* **2006**, *128*, 9008–9009. (i) Ueki, S.; Sahlan, M.; Ishida, T.; Nogami, T. *Synth. Met.* **2005**, *154*, 217. (j) Mori, F.; Ishida, T.; Nogami, T. *Polyhedron* **2005**, *24*, 2588. (k) Aronica, C.; Pilet, G.; Chastanet, G.; Wernsdorfer, W.; Jacquot, J.-P.; Luneau, D. *Angew. Chem., Int. Ed.* **2006**, *45*, 4659–4662. (l) Pointillart, F.; Bernot, K.; Sessoli, R.; Gatteschi, D. *Chem.—Eur. J.* **2007**, *13*, 1602–1609. (m) He, F.; Tong, M.-L.; Chen, X.-M. *Inorg. Chem.* **2005**, *44*, 8285–8292. (n) Mereacre, V. M.; Ako, A. M.; Clérac, R.; Wernsdorfer, W.; Filoti, G.; Bartolomé, J.; Anson, C. E.; Powell, A. K. *J. Am. Chem. Soc.* **2007**, *129*, 9248–9249. (o) Hamamatsu, T.; Yabe, K.; Towatari, M.; Matsumoto, N.; Re, N.; Pochaba, A.; Mrozinlski, J. *Bull. Chem. Soc. Jpn.* **2007**, *80*, 523–529.

(5) (a) Caneschi, A.; Gatteschi, D.; Lalioti, N.; Sangregorio, C.; Sessoli, R.; Venturi, G.; Vindigni, A.; Rettori, A.; Pini, M. G.; Novak, M. A. *Angew. Chem., Int. Ed.* **2001**, *40*, 1760–1763. (b) Clérac, R.; Miyasaka, H.; Yamashita, M.; Coulon, C. *J. Am. Chem. Soc.* **2002**, *124*, 12837–12844. (c) Miyasaka, H.; Clérac, R. *Bull. Chem. Soc. Jpn.* **2005**, *78*, 1725–1748. (d) Saitoh, A.; Miyasaka, H.; Yamashita, M.; Clérac, R. *J. Mater. Chem.* **2007**, *17*, 2002–2012. (e) Costes, J.-P.; Clemente-Juan, J. M.; Dahan, F.; Milon, J. *Inorg. Chem.* **2004**, *43*, 8200–8202. (f) Bernot, K.; Bogani, L.; Caneschi, A.; Gatteschi, D.; Sessoli, R. *J. Am. Chem. Soc.* **2006**, *128*, 7947–7956. (g) Bogani, L.; Sangregorio, C.; Sessoli, R.; Gatteschi, D. *Angew. Chem., Int. Ed.* **2005**, *44*, 5817–5821.

Table 1. Crystallographic Data for H_3L, [(NiL)Eu(hfac)$_2$(EtOH)]·EtOH (**1·Eu**), [(NiL)Gd(hfac)$_2$(EtOH)]·1.5EtOH (**1·Gd**), [(NiL)Tb(hfac)$_2$(EtOH)]·EtOH·H_2O (**1·Tb**), and [(NiL)Dy(hfac)$_2$(EtOH)]·EtOH·H_2O (**1·Dy**)

	H_3L	**1·Eu**	**1·Gd**	**1·Tb**	**1·Dy**
formula	$C_{26}H_{27}N_3O_3$	$C_{40}H_{38}EuF_{12}N_3NiO_9$	$C_{41}H_{41}F_{12}GdN_3NiO_{9.5}$	$C_{40}H_{40}F_{12}N_3NiO_{10}Tb$	$C_{40}H_{40}DyF_{12}N_3NiO_{10}$
fw	429.52	1143.40	1171.72	1168.38	1171.95
cryst syst	monoclinic	triclinic	triclinic	triclinic	triclinic
space group	$P2_1/c$ (No. 14)	$P\bar{1}$ (No. 2)	$P\bar{1}$ (No. 2)	$P\bar{1}$ (No. 2)	$P\bar{1}$ (No. 2)
a/Å	5.8092(3)	13.2218(2)	12.852(3)	12.8622(12)	12.814(4)
b/Å	23.2124(5)	13.3279(3)	13.433(3)	13.3803(13)	13.404(5)
c/Å	16.6598(4)	13.7567(3)	14.899(4)	14.8945(15)	14.868(5)
α/deg	90	86.911(4)	83.622(10)	83.752(2)	83.612(14)
β/deg	93.403(2)	77.108(5)	64.537(10)	64.7225(18)	64.495(12)
γ/deg	90	71.8634(11)	87.905(9)	88.102(2)	87.906(12)
V/Å^3	2242.54(14)	2245.36(8)	2307.7(9)	2303.9(4)	2290.3(13)
Z	4	2	2	1.684	1.699
D_{calc}/g cm^{-3}	1.272	1.691	1.686	2	2
μ/cm^{-1}	0.841	19.051	19.410	20.330	21.381
R_1[a] [$I > 2\sigma(I)$]	0.0395	0.0550	0.0309	0.0402	0.0429
wR_2[b] [all data]	0.0878	0.1370	0.0813	0.1100	0.1294
T/°C	−180(1)	−50(1)	−170(1)	−180(1)	−180(1)

[a] $R_1 = \sum||F_o| - |F_d||/\sum|F_o|$. [b] $wR_2 = [\sum w(|F_o^2| - |F_c^2|)^2/\sum w|F_o^2|^2]^{1/2}$.

$[Ni(H_{1.5}L)]Cl_{0.5}$ (**1**).[10] In the $Ni^{II}-M^{II}-Ni^{II}$ complex, each terminal high-spin Ni^{II} unit is coordinated by the L^{3-} ligand in an octahedral fashion and functions as a tridentate ligand, and the central M^{II} ion is bridged by six phenolate oxygen atoms to the terminal Ni^{II} ions. By using $[NiL]^-$ as the complex ligand by replacing the central M^{II} ion with a Gd^{III} ion, we could prepare a dinuclear mixed $Ni^{II}-Gd^{III}$ complex.[7] Preparation of desired 3d−4f complexes is usually difficult because of the lability of the Ln^{III} ion. Thus, the employment of the complexes-as-ligands strategy should be the right way to construct 3d−4f complexes. The reaction of $[Ni(H_{1.5}L)]Cl_{0.5}$ (**1**), $[Ln(hfac)_3(H_2O)_2]$, and triethylamine in ethanol (1:1:1) afforded [(NiL)Ln(hfac)$_2$(EtOH)]·nEtOH·mH$_2$O (**1·Ln**; $n = 1$ or 1.5; $m = 0$ or 1). The crystals of **1·Gd**, **1·Tb**, and **1·Dy** are isomorphous and dichroic (yellow and pink), while those of **1·Eu** are pale yellow. The coordinated ethanol molecule and solvent molecules of crystallization are easily lost upon drying. Although we tried the reaction of **1** with $[Gd(hfac)_3(H_2O)_2]$ in different molar ratios, 1:1, 2:1, and 3:1, in the hope of synthesizing the $Ni^{II}-Gd^{III}-Ni^{II}$-type trinuclear complex, we always obtained the same product, **1·Gd**. Because $hfac^-$ ligands on Gd^{III} are bulky and not very labile, they prevent a second $[NiL]^-$ unit from coordinating, and the $Ni^{II}-Gd^{III}$-type dinuclear complex (**1·Gd**) was always formed.

Table 2. Coordinate Bond Lengths (Å) and Ln···Ni Distances (Å) with Their Estimated Standard Deviations in Parentheses for [(NiL)Eu(hfac)$_2$(EtOH)]·EtOH (**1·Eu**), [(NiL)Gd(hfac)$_2$(EtOH)]·1.5EtOH (**1·Gd**), [(NiL)Tb(hfac)$_2$(EtOH)]·EtOH·H_2O (**1·Tb**), and [(NiL)Dy(hfac)$_2$(EtOH·H_2O)]·EtOH·H_2O (**1·Dy**)

	1·Eu	**1·Gd**	**1·Tb**	**1·Dy**
Ln(1)−O(1)	2.330(3)	2.3106(17)	2.292(2)	2.284(2)
Ln(1)−O(2)	2.373(4)	2.4020(16)	2.372(2)	2.383(4)
Ln(1)−O(3)	2.375(4)	2.3637(16)	2.336(2)	2.332(3)
Ln(1)−O(4)	2.419(6)	2.3735(18)	2.356(2)	2.345(3)
Ln(1)−O(5)	2.473(4)	2.4023(18)	2.379(2)	2.384(3)
Ln(1)−O(6)	2.468(5)	2.4567(17)	2.439(3)	2.430(4)
Ln(1)−O(7)	2.418(5)	2.3954(17)	2.380(2)	2.369(3)
Ln(1)−O(8)	2.441(5)	2.4010(18)	2.393(2)	2.390(3)
Ni(1)−O(1)	2.113(5)	2.0994(16)	2.090(3)	2.097(4)
Ni(1)−O(2)	2.080(3)	2.0809(17)	2.077(2)	2.074(3)
Ni(1)−O(3)	2.108(4)	2.0647(16)	2.066(2)	2.069(2)
Ni(1)−N(1)	2.059(5)	2.049(2)	2.050(2)	2.035(3)
Ni(1)−N(2)	2.051(6)	2.032(2)	2.033(3)	2.031(4)
Ni(1)−N(3)	2.054(6)	2.058(2)	2.055(4)	2.055(5)
Ln(1)···Ni(1)	3.1873(7)	3.1617(9)	3.1432(4)	3.1380(6)

Figure 1b shows the molecular structure of the H_3L ligand as determined by single-crystal X-ray diffraction analysis. The crystallographic data are summarized in Table 1. The three arms spread out, and each phenolic hydrogen atom is linked to the imine nitrogen atom in the same arm, with an average O···N distance of 2.59 Å. Selected bond lengths and angles with their estimated standard deviations in parentheses are listed in Table S1 (Supporting Information). The preparation and the structure of $[Ni(H_{1.5}L)]Cl_{0.5}$·MeOH (**1**) is reported elsewhere.[10] The Ni^{II} ion of **1** is in an approximately octahedral environment composed of three facially coordinated imine nitrogen atoms and three phenolate oxygen atoms, as shown in Figure 1c.

All **1·Ln** complexes (**1·Eu**, **1·Gd**, **1·Tb**, and **1·Dy**) crystallized in the triclinic space group $P\bar{1}$ (No. 2) with $Z = 2$. The crystallographic data are listed in Table 1. Coordinate bond lengths and Ln···Ni distances with their estimated standard deviations in parentheses are listed in Table 2. All complexes have similar structures, and Figure 2 shows the molecular structure of **1·Gd** as a representative example. The complex is a face-sharing dinuclear molecule, and the Ni···Gd distance is 3.1617(9) Å. The Ni^{II} ion is coordinated by the L^{3-} ligand in a N_3O_3 coordination sphere. The three

(6) (a) Sugita, M.; Ishikawa, N.; Koshihara, E.; Kaizu, Y. *Inorg. Chem.* **2006**, *45*, 1299–1304. (b) Ishikawa, N.; Sugita, M.; Tanaka, N.; Ishikawa, T.; Koshihara, S.; Kaizu, Y. *Inorg. Chem.* **2004**, *43*, 5498–5500. (c) Ishikawa, N.; Sugita, M.; Wernsdorfer, W. *J. Am. Chem. Soc.* **2005**, *127*, 3650–3651. (d) Ishikawa, N.; Iino, T.; Kaizu, Y. *J. Phys. Chem. A* **2002**, *106*, 9543–9550. (e) Ishikawa, N.; Iino, T.; Kaizu, Y. *J. Am. Chem. Soc.* **2002**, *124*, 11440–11447. (f) Ishikawa, N.; Sugita, M.; Okubo, T.; Tanaka, N.; Iino, T.; Kaizu, Y. *Inorg. Chem.* **2003**, *42*, 2440–2446.

(7) Yamaguchi, T.; Sunatsuki, Y.; Kojima, M.; Akashi, H.; Tsuchimoto, M.; Re, N.; Osa, S.; Matsumoto, N. *Chem. Commun.* **2004**, 1048–1049.

(8) (a) Ohta, H.; Harada, K.; Irie, K.; Kashino, S.; Kambe, T.; Sakane, G.; Shibahara, T.; Takamizawa, S.; Mori, W.; Nonoyama, M.; Hirotsu, M.; Kojima, M. *Chem. Lett.* **2001**, 842–843. (b) Kojima, M.; Ohta, H. *Monogr. Ser. Int. Conf. Coord. Chem.* **2001**, *5*, 65–70.

(9) Kobayashi, T.; Yamaguchi, T.; Ohta, H.; Sunatsuki, Y.; Kojima, M.; Re, N.; Nonoyama, M.; Matsumoto, N. *Chem. Commun.* **2006**, 1950–1952.

(10) Yamaguchi, T.; Sunatsuki, Y.; Ishida, H. *Acta Crystallogr., Sect. C* **2008**, *64*, m156–m160.

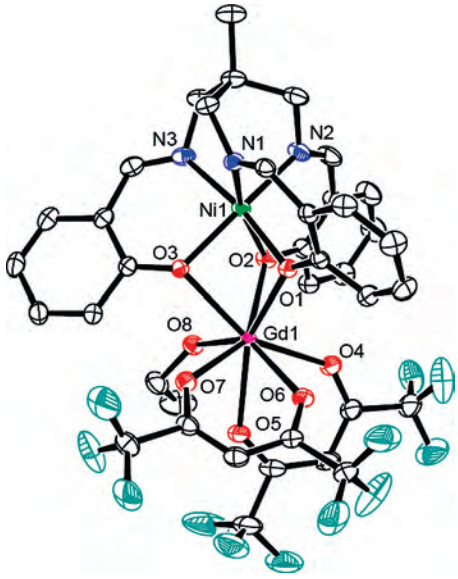

Figure 2. ORTEP drawing of [(NiL)Gd(hfac)$_2$(EtOH)]·1.5EtOH (**1·Gd**), showing atom numbering and 50% probability displacement ellipsoids. The hydrogen atoms and solvent molecules of crystallization are omitted for clarity.

phenolate oxygen atoms coordinate to a Gd^{III} ion as bridging atoms, with an average Gd−O bond length of 2.36 Å. The Gd^{III} ion is eight-coordinate, with four oxygen atoms of two hfac$^-$'s, three phenolate oxygen atoms of L^{3-}, and one ethanol oxygen atom coordinated. The coordination bond lengths around the Ni^{II} ion are very similar among the **1·Ln** complexes (Table 2). Upon complexation with an Ln^{III} ion, the Ni−O bond lengths increase a little compared with those of **1**, while the Ni−N bond lengths decrease a little. The average of eight Ln−O bond lengths decreases as the atomic number increases in accordance with the lanthanide contraction: **1·Eu**, 2.41 Å; **1·Gd**, 2.39 Å; **1·Tb**, 2.38 Å; **1·Dy**, 2.37 Å (Table 2). Concomitantly, the Ln···Ni distance decreases in the order 3.1873(7) Å (**1·Eu**) > 3.1617(9) Å (**1·Gd**) > 3.1432(4) Å (**1·Tb**) > 3.1380(6) Å (**1·Dy**). Figure 3 shows the crystal structure of **1·Gd**. The benzene rings of the L^{3-} ligands in neighboring molecules are stacked with a spacing of ca. 3.5 Å to form a chain structure along the *b* axis. A similar chain structure is observed in all **1·Ln** complexes, although the chain runs along the *c* axis in **1·Eu**. The smallest distances between the metal ions in **1·Gd** are Gd···Gd = 9.46051(12) Å, Ni···Ni = 7.4274(4) Å, and Gd···Ni = 7.8954(2) Å [**1·Eu**: Eu···Eu = 9.6805(3) Å, Ni···Ni = 7.4302(11) Å, and Eu···Ni = 8.0188(7) Å; **1·Tb**: Tb···Tb = 9.42928(16) Å, Ni···Ni = 7.4072(6) Å, and Tb···Ni = 7.8746(4) Å; **1·Dy**: Dy···Dy = 9.4077(3) Å, Ni···Ni = 7.3801(8) Å, and Dy···Ni = 7.8510(5) Å].

In order to investigate the magnetic properties of **1·Ln** (Ln = Eu, Tb, Dy) with the complicating effect of spin−orbit coupling, we have prepared the analogous Zn(II)−Ln(III) complexes, [(ZnL)Ln(hfac)$_2$(EtOH)]·EtOH (**2·Ln**) as reference complexes. The preparation and the structure of [Zn(H$_{1.5}$L)](ClO$_4$)$_{0.5}$·1.5MeOH (**2**) is reported elsewhere.[10] The complex may be formulated as [Zn(H$_2$L)][Zn(HL)]-ClO$_4$·3MeOH.

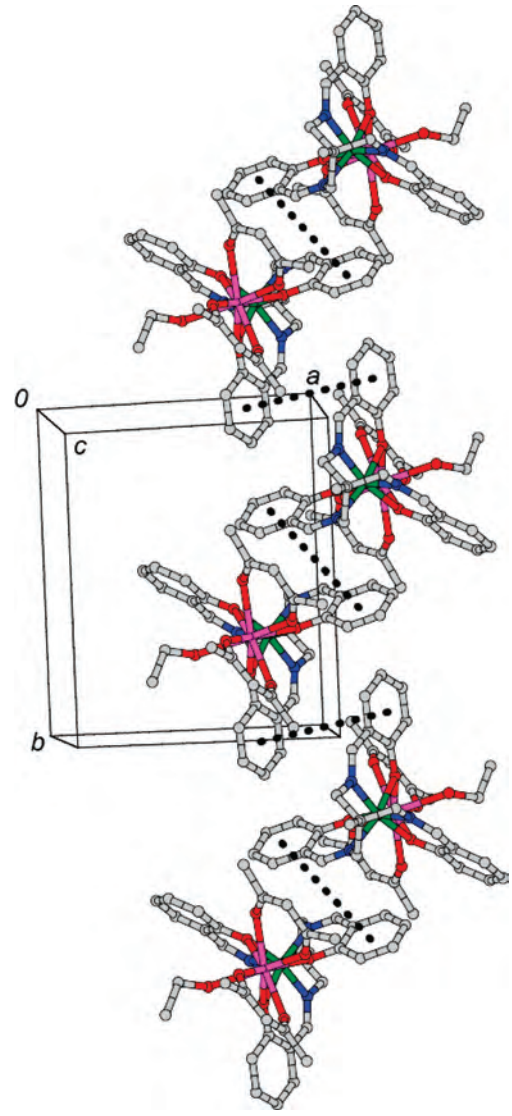

Figure 3. Crystal structure of [(NiL)Gd(hfac)$_2$(EtOH)]·1.5EtOH (**1·Gd**). The neighboring benzene rings of the L^{3-} ligands are stacked with a spacing of ca. 3.5 Å to form a chain structure along the *b* axis. The dotted lines show the stacking of the benzene rings. The hydrogen and fluorine atoms and crystal solvents are omitted for clarity.

Heterodinuclear Zn−Ln complexes ([(ZnL)Ln(hfac)$_2$-(EtOH)]·EtOH (**2·Ln**)), the Zn analog of **1·Ln**, were prepared by the reaction of **2**, [Ln^{III}(hfac)$_3$(H$_2$O)$_2$], and triethylamine (1:1:3) in ethanol. All of the complexes, **2·Eu**, **2·Gd**, **2·Tb**, and **2·Dy**, crystallized in the triclinic space group $P\bar{1}$ (No. 2) with $Z = 2$. The crystallographic data are listed in Table 3. Coordinate bond lengths and Ln···Zn distances with their estimated standard deviations in parentheses are listed in Table 4. The molecular structures are very similar to each other, and the structure of **2·Gd** is shown in Figure S1 (Supporting Information) as a representative example. Upon complexation with a Ln^{III} ion, the Zn−O bond lengths increase compared with those of **2**, while the Zn−N bond lengths decrease. We compared the structural parameters of **2·Gd** with those of **1·Gd**: for **1·Gd**, Ni−O(av.) = 2.082 Å, Ni−N(av.) = 2.046 Å, Gd−O(av.) = 2.388 Å, Ni···Gd = 3.1617(9) Å; for **2·Gd**, Zn−O(av.) = 2.141 Å, Zn−N(av.) = 2.119 Å, Gd−O(av.) = 2.395 Å,

Table 3. Crystallographic Data for [(ZnL)Eu(hfac)$_2$(EtOH)]·EtOH (**2·Eu**), [(ZnL)Gd(hfac)$_2$(EtOH)]·EtOH (**2·Gd**), [(ZnL)Tb(hfac)$_2$(EtOH)]·EtOH (**2·Tb**), and [(ZnL)Dy(hfac)$_2$(EtOH)]·EtOH (**2·Dy**)

	2·Eu	**2·Gd**	**2·Tb**	**2·Dy**
formula	$C_{40}H_{38}EuF_{12}N_3O_9Zn$	$C_{40}H_{38}F_{12}GdN_3O_9Zn$	$C_{40}H_{38}F_{12}N_3O_9TbZn$	$C_{40}H_{38}DyF_{12}N_3O_9Zn$
fw	1150.08	1155.37	1157.04	1160.62
cryst syst	triclinic	triclinic	triclinic	triclinic
space group	$P\bar{1}$ (No. 2)	$P\bar{1}$ (No. 2)	$P\bar{1}$ (No. 2)	$P\bar{1}$ (No. 2)
a/Å	12.903(2)	12.9143(6)	12.9382(8)	12.9821(10)
b/Å	13.384(2)	13.3824(6)	13.3429(10)	13.3367(10)
c/Å	13.4859(13)	13.4886(3)	13.4663(10)	13.4718(5)
α/deg	86.260(8)	86.0347(19)	85.906(3)	85.778(3)
β/deg	78.067(9)	77.898(2)	77.6875(12)	77.426(4)
γ/deg	71.286(3)	71.1947(8)	71.272(3)	71.3317(13)
V/Å^3	2158.2(5)	2157.67(15)	2151.0(3)	2156.8(2)
Z	2	2	2	2
D_{calc}/g cm^{-3}	1.770	1.778	1.786	1.787
μ/cm^{-1}	21.016	21.929	22.944	23.871
R_1[a] [$I > 2\sigma(I)$]	0.0409	0.0367	0.0686	0.0517
wR_2[b] [all data]	0.1209	0.1020	0.1723	0.1331
T/°C	−180(1)	−150(1)	−180(1)	−150(1)

[a] $R_1 = \sum||F_o| - |F_c||/\sum|F_o|$. [b] $wR_2 = [\sum w(|F_o^2| - |F_c^2|)^2/\sum w|F_o^2|^2]^{1/2}$.

Table 4. Coordinate Bond Lengths (Å) and Ln···Zn Distances (Å) with Their Estimated Standard Deviations in Parentheses for [(ZnL)Eu(hfac)$_2$(EtOH)]·EtOH (**2·Eu**), [(ZnL)Gd(hfac)$_2$(EtOH)]·EtOH (**2·Gd**), [(ZnL)Tb(hfac)$_2$(EtOH)]·EtOH (**2·Tb**), and [(ZnL)Dy(hfac)$_2$(EtOH)]·EtOH (**2·Dy**)

	2·Eu	**2·Gd**	**2·Tb**	**2·Dy**
Ln(1)−O(1)	2.318(2)	2.304(2)	2.308(3)	2.283(2)
Ln(1)−O(2)	2.372(2)	2.363(2)	2.346(4)	2.325(2)
Ln(1)−O(3)	2.371(3)	2.371(2)	2.348(5)	2.340(3)
Ln(1)−O(4)	2.414(3)	2.407(3)	2.388(5)	2.372(4)
Ln(1)−O(5)	2.478(2)	2.466(2)	2.462(4)	2.443(2)
Ln(1)−O(6)	2.467(3)	2.457(2)	2.437(5)	2.433(3)
Ln(1)−O(7)	2.407(3)	2.383(2)	2.387(5)	2.354(3)
Ln(1)−O(8)	2.421(2)	2.408(2)	2.397(4)	2.386(3)
Zn(1)−O(1)	2.162(3)	2.173(2)	2.166(4)	2.166(3)
Zn(1)−O(2)	2.120(2)	2.118(2)	2.121(4)	2.124(2)
Zn(1)−O(3)	2.129(2)	2.131(2)	2.129(4)	2.124(3)
Zn(1)−N(1)	2.131(3)	2.119(2)	2.130(4)	2.122(3)
Zn(1)−N(2)	2.118(3)	2.111(3)	2.108(5)	2.100(3)
Zn(1)−N(3)	2.127(4)	2.127(3)	2.131(6)	2.121(4)
Ln(1)···Zn(1)	3.2250(4)	3.2177(3)	3.2080(7)	3.1925(5)

Zn···Gd = 3.2177(3) Å. The coordinate bond lengths around Ni are smaller than those for Zn by about 0.05 Å, in accordance with the smaller ionic radius of Ni compared with Zn, and the Gd−O(av.) lengths in **1·Gd** and **2·Gd** are almost the same. Complexes **1·Eu** and **2·Eu** are crystallographically isomorphous, and all other complexes **1·Ln** (Ln = Gd, Tb, Dy) and **2·Ln** are not crystallographically isomorphous to each other. However, their structures are closely related and can be regarded as isostructural. Thus, we conclude that we can use **2·Ln** as reference molecules in studying the magnetic properties of **1·Ln**.

Magnetic Properties of Ni^{II}Ln^{III} (1·Ln) and Zn^{II}Ln^{III} (2·Ln). Both **1·Ln** and **2·Ln** are efflorescent, and they easily lose the coordinated ethanol molecule and solvent molecules of crystallization. The samples we used for magnetic measurements are formulated as [(NiL)Ln(hfac)$_2$] and [(ZnL)Ln(hfac)$_2$] (see Experimental Section). Temperature-dependent molar susceptibility measurements of powdered samples of **1·Ln** were carried out in an applied field of 0.1 T in the temperature range 1.9−300 K. The data are presented as plots of $\chi_M T$ versus T in Figure 4, where χ_M is the molar magnetic susceptibility and T is the absolute temperature. The $\chi_M T$ value of **1·Gd** is 8.74 cm^3 K mol^{-1} at 300 K, in line with the value of 8.88 cm^3 K mol^{-1} expected for Ni^{II} ($S = 1$) and Gd^{III} (4f^7, $J = 7/2$, $L = 0$, $S = 7/2$, $^8S_{7/2}$) noninteracting ions. The profile of the curve for **1·Gd** shows a steady increase upon reducing the temperature, indicating that the overall magnetic interaction between the metal ions is ferromagnetic. The maximum value of $\chi_M T$, 11.1 cm^3 K mol^{-1} at 1.9 K, is slightly lower than the value of 12.37 cm^3 K mol^{-1} expected for an isolated $S = 9/2$ spin resulting from ferromagnetic coupling between the Ni^{II} ($S = 1$) and Gd^{III} ($S = 7/2$) ions of the dinuclear complex. Fits to the experimental data were performed assuming for the Gd^{III} ion an isotropic $^8S_{7/2}$ state without orbital angular momentum and using the following spin Hamiltonian, $\mathbf{H} = g\beta(\mathbf{S}_{Ni} + \mathbf{S}_{Gd})H + D_{Ni}[\mathbf{S}_{Niz}^2 - S(S+1)/3] + 2J\,\mathbf{S}_{Ni}\cdot\mathbf{S}_{Gd}$ in which g is an average g factor for the Gd^{III} and Ni^{II} ions, H is the applied field, D_{Ni} is the ZFS parameter for Ni^{II}, and J is the Heisenberg coupling constant between the two ions. The inclusion of the ZFS term is consistent with the analysis of the magnetization data (see below) and allows an improved fit at low temperatures.[11] The best-fit parameters to the data were $g = 2.15$, J(Ni−Gd) = +0.34 cm^{-1}, and $D = +1.5$ cm^{-1}. The calculated J(Ni−Gd) value is lower than that

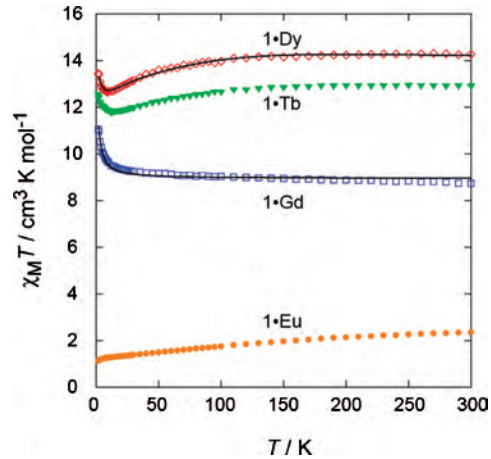

Figure 4. Magnetic behaviors of [(NiL)Eu(hfac)$_2$] (**1·Eu**, ●), [(NiL)Gd(hfac)$_2$] (**1·Gd**, □), [(NiL)Tb(hfac)$_2$] (**1·Tb**, ▼), and [(NiL)Dy(hfac)$_2$] (**1·Dy**, ◊) in the form of $\chi_M T$ vs T plots in the temperature range 1.9−300 K. The solid lines correspond to the best data fits for **1·Dy** and **1·Gd**.

reported by Costes et al. for a $Gd^{III}-Ni^{II}$ dinuclear complex with two phenoxo bridges of $J = +3.6$ cm^{-1},[12] but it is similar to the value observed by Chen et al. for a $Gd^{III}-Ni^{II}$ compound with three phenoxo bridges, which had $J = +0.56$ cm^{-1}.[13]

The field dependence of the magnetization for **1·Gd** was also measured at 2 K, and the *M* versus *H* curve is shown in Figure S2 (Supporting Information). The data are qualitatively reproduced by Brillouin curves for $S = 9/2$, demonstrating that the spin ground state is derived from the ferromagnetic coupling between Ni^{II} ($S = 1$) and Gd^{III} ($S = 7/2$) ions. The data are well-simulated (see the solid line in Figure S2, Supporting Information) including ZFS for the same spin systems, and the best fit to the experimental data yields the following values: $g = 2.21$ and $D = +0.22$ cm^{-1}. It is worth noting that the *D* value obtained from the fit of the magnetization data refers to the $S = 9/2$ state and can be compared with the single ion values for Ni^{II} obtained from a fit of the magnetic susceptibility using the Wigner−Eckart theorem.[14] For instance, using eqs 6.4.3 and 6.4.4 of ref 14 and taking into account that the ZFS of the Gd^{III} ion is negligible, it can be shown that $D_{9/2} = (1/36)D_{Ni(II)}$. This justifies, at least qualitatively, the smaller value of *D*, by 1 order of magnitude, obtained from the fit of the magnetization data.

Temperature-dependent molar susceptibility measurements of powdered samples of **2·Ln** were carried out under the same conditions as for **1·Ln**. The data are presented as plots of $\chi_M T$ versus *T* in Figure S3 (Supporting Information). The magnetic properties of **1·Eu**, **1·Tb**, and **1·Dy** are difficult to investigate because of the orbital contribution. Figure 5 shows the temperature-dependent molar susceptibility of **1·Dy** and the isostructural $[(Zn^{II}L)Dy^{III}(hfac)_2]$ complex (**2·Dy**) as a reference compound involving the diamagnetic Zn^{II} ion. The $\chi_M T$ value of 14.28 cm^3 K mol^{-1} at 300 K for **1·Dy** is compatible with the calculated value of 15.17 cm^3 K mol^{-1} for independent Ni^{II} ($S = 1$) and Dy^{III} ($4f^9$, $J = 15/2$, $S = 5/2$, $L = 5$, $^6H_{15/2}$), and the $\chi_M T$ value decreases gradually with decreasing temperature to 12.64 cm^3 K mol^{-1} at 9.0 K but then increases at lower temperatures, reaching a maximum value of 13.46 cm^3 K mol^{-1} at 1.9 K. The $\chi_M T$ value of **2·Dy** decreases gradually from 13.35 cm^3 K mol^{-1} at 300 K to 10.88 cm^3 K mol^{-1} at 1.9 K. The nature of the magnetic interaction between Ni^{II} and Dy^{III} was investigated by an empirical approach developed by Costes et al.[15] and Kahn et al.[16] The difference between the $\chi_M T$ values for the $Ni^{II}Dy^{III}$ complex and the $Zn^{II}Dy^{III}$ complex, $\Delta(T) = (\chi_M T)_{NiDy} - (\chi_M T)_{ZnDy} = (\chi_M T)_{Ni} + J_{NiDy}(T)$, where $(\chi_M T)_{Ni}$ is the

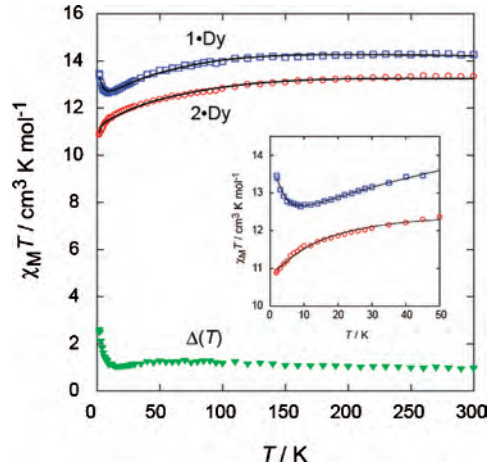

Figure 5. Plots of $\chi_M T$ vs *T* for $[(NiL)Dy(hfac)_2]$ (**1·Dy**, □) and $[(ZnL)Dy(hfac)_2]$ (**2·Dy**, ○), and the difference $\Delta(T) = (\chi_M T)_{NiDy} - (\chi_M T)_{ZnDy} = (\chi_M T)_{Ni} + J_{NiDy}(T)$ (▼). The solid lines correspond to the best data fits. Inset shows the $\chi_M T$ vs *T* plots in the temperature range 2−50 K and the best data fits (solid lines) obtained from the analysis of the magnetic susceptibility in this temperature range (see text).

$\chi_M T$ value attributable to an isolated Ni^{II} ion, 1.0 cm^3 K mol^{-1}, and the temperature-dependent contribution $J_{NiDy}(T)$ is related to the nature of the overall exchange interactions between the Ni^{II} and Dy^{III} ions; a positive or a negative value being directly related to a ferro- or antiferromagnetic interaction, respectively, is also plotted in Figure 5. The $\Delta(T)$ value is almost constant (1.1−1.2 cm^3 K mol^{-1}) over the whole temperature range, except for an increase in the lowest-temperature region. The profile of the $\Delta(T)$ plots with its increase at low temperatures indicates a ferromagnetic interaction between Ni^{II} and Dy^{III}. The magnetic properties of **1·Tb** and **1·Eu** were studied in the same way. The difference, $\Delta(T)$, between the $\chi_M T$ values for the $Ni^{II}Tb^{III}$ complex (**1·Tb**) and the $Zn^{II}Tb^{III}$ complex (**2·Tb**) and that between the $\chi_M T$ values for the $Ni^{II}Eu^{III}$ complex (**1·Eu**) and the $Zn^{II}Eu^{III}$ complex (**2·Eu**) are shown in Figures S4 and S5 (Supporting Information), respectively. For the Tb^{III} complexes, the $\Delta(T)$ value is larger than 1.0 cm^3 K mol^{-1} over the entire temperature region and increases below 30 K, indicating a ferromagnetic interaction between Ni^{II} and Tb^{III} (Figure S4, Supporting Information). In the case of Eu^{III} complexes, the $\Delta(T)$ value is almost constant (1.17−1.23 cm^3 K mol^{-1}) down to 6 K. Below 6 K, the $\Delta(T)$ value decreases a little (1.10 cm^3 K mol^{-1} at 1.9 K; Figure S5, Supporting Information). From these results, we conclude that the interaction between Ni^{II} and Eu^{III} is negligible. Very recently, Dunbar et al.[17] studied the magnetic interaction between Sm^{III} and low-spin Fe^{III} by comparing the χT curve with those of the isostructural $Sm^{III}-Co^{III}$ and $La^{III}-Fe^{III}$ compounds.

To gain insight into the sublevel structure of the Dy^{III} ion and its coupling with Ni^{II}, we analyzed in detail the magnetic behavior of **1·Dy** and **2·Dy**. The ground state for a Dy^{III} ion is $^6H_{15/2}$, with $g_J = 4/3$, separated by more than 1500 cm^{-1} from the first excited state, $^6H_{13/2}$. Indeed, the room-

(11) We also performed the fittings taking interactions between the adjacent molecules into account. The results revealed that the intermolecular interactions are very small.

(12) Costes, J.-P.; Dahan, F.; Dupuis, A.; Laurent, J.-P. *Inorg. Chem.* **1997**, *36*, 4284–4286.
(13) Chen, Q.-Y.; Luo, Q.-H.; Zheng, L.-M.; Wang, Z.-L.; Chen, J.-T. *Inorg. Chem.* **2002**, *41*, 605–609.
(14) Kahn, O. *Molecular Magnetism*; VCH: Weinheim, Germany, 1993; section 6.4 and references therein.
(15) Costes, J.-P.; Dahan, F.; Dupuis, A.; Laurent, J.-P. *Chem.—Eur. J.* **1998**, *4*, 1616–1620.
(16) Kahn, M. L.; Mathoniere, C.; Kahn, O. *Inorg. Chem.* **1999**, *38*, 3692–3697.
(17) Zhao, H.; Lopez, N.; Prosvirin, A.; Chifotides, H.; Dunbar, K. R. *Dalton Trans.* **2007**, 878–888.

temperature value of $\chi_M T$ for **2·Dy** is in good agreement with the free ion value 14.17 cm^3 K mol^{-1} obtained using the total angular momentum $J = 15/2$ and the above g_J factor. However, the $^6H_{15/2}$ state is partially split by the ligand field into a series of Stark sublevels whose width is on the order of 100 cm^{-1}. Therefore, at room temperature, most sublevels are populated and the free ion value is approached; when the temperature is decreased, the depopulation of the higher sublevels leads to a deviation from the Curie law, as observed in a decrease of $\chi_M T$ even in the absence of any exchange interaction. A detailed analysis of the crystal field effect on the $\chi_M T$ product for **2·Dy** would require the diagonalization of a spin Hamiltonian, $\mathbf{H} = g\beta(\mathbf{L} + 2\mathbf{S})H + \mathbf{H}_{cf}$, including the crystal field interaction contribution, $\mathbf{H}_{cf}$, several terms up to the sixth order (the exact number depending on the coordination symmetry) in Steven's operator:[18]

$$\mathbf{H}_{cf} = \sum_{k=2,4,6} \sum_{q=0}^{k} B_k^q \mathbf{O}_k^q \qquad (1)$$

A Hamiltonian including explicitly this contribution has been used to interpret the magnetic properties and the optical and EPR spectra of lanthanide compounds by physicists since the 1950s (see, for instance, ref 18 and references therein) and also more recently employed in the chemistry community to describe the magnetic behavior of lanthanide complexes.[19–23] The $\chi_M T$ versus T curve for **2·Dy** could be accurately reproduced considering only the lowest $^6H_{15/2}$ term and including only the $\mathbf{O}_2^2$ and $\mathbf{O}_2^0$ contributions, the ZFS, and the rhombic distortion terms (see ref 18, section 3.5), that is, using the simpler spin Hamiltonian:

$$\mathbf{H} = g\beta\mathbf{J}H + D\left[\mathbf{J}_z^2 - J(J+1)/3\right] + E\left(\mathbf{J}_x^2 - \mathbf{J}_y^2\right) \qquad (2)$$

in which g is an empirical g factor (hopefully close to g_J), $J = 15/2$ is the total angular momentum, H is the applied field, D is the ZFS parameter, and E is the rhombic distortion parameter for the Dy^{III} ion. A good fit was obtained in the whole temperature range of 2−300 K ($g = 1.27$, $D = -6.5$ cm^{-1}, and $E = -0.8$ cm^{-1}; see solid line in Figure 5 and Figure S3, Supporting Information). However, a more accurate analysis of the magnetic susceptibility was performed in the low-temperature range, where only the lowest Stark sublevels are populated and the fitting is more valid and directly comparable with the low-temperature magnetization data. Best fits were performed for several ranges, starting from 2 to 100 K and decreasing the maximum temperature, and for the ranges below 50 K (2−20, 2−30, 2−40, and 2−50 K), the fits gave almost constant results with the D and E parameters that are significantly lower than the values obtained from the fit in the whole temperature range 2−300 K. For the 2−50 K range, the best fit parameters are $g = 1.25$, $D = -2.0$ cm^{-1}, and $E = -0.7$ cm^{-1}, see the solid line in the inset of Figure 5, showing that the value of D obtained from the high temperature fit, -6.5 cm^{-1}, is overestimated. It is worth noting that, with the D and E parameters determined as described above, the lowest of the 16 sublevels into which the $^6H_{15/2}$ state is split are $|+15/2\rangle$ and $|-15/2\rangle$ with the next $|+13/2\rangle$ and $|-13/2\rangle$ levels lying at about 40 cm^{-1} and the highest (mainly a combination of $|\pm1/2\rangle$ and $|\pm5/2\rangle$ states) ca. 170 cm^{-1} above (see Scheme 1). The $|\pm15/2\rangle$ levels are therefore the only substates to be populated below 10 K, thus determining a strong Ising-type anisotropy of the Dy^{III} ion at low temperatures. The values of D and E and the corresponding energy splitting of the Stark sublevels found for **2·Dy** are qualitatively similar to those recently evaluated for some mono- and polynuclear Dy complexes with phthalocyanines and terpyridine ligands.[6d–f,23] In these studies, another set of parameters, $A_k^q\langle r^k\rangle$, are actually used. They are easily transformed into the B_k^q set using the formula $B_k^q = A_k^q\langle r^k\rangle\langle J||\alpha_k||J\rangle$, where the last factors are the operator-equivalent coefficients relating the angular momentum operators to the potential operators, whose values are reported in ref 18. The sets of $A_k^q\langle r^k\rangle$ values for the Dy complexes reported in these studies, $A_2^0\langle r^2\rangle$ in the range 150−500 cm^{-1} and fourth- and sixth-order terms below 500 cm^{-1},[6d–f] are easily transformed into B_2^0, that is, $D = 3B_2^0$ values of -1.5 to -4.5 cm^{-1}, very close to the value of -2.0 cm^{-1} found for **2·Dy**, and in B_4^q and B_6^q, values are more than 2 orders of magnitude smaller, in agreement with our assumption to neglect them (a zero B_2^2, i.e. E, was assumed in refs 6d–f for those axially symmetric complexes), see Supporting Information Appendix A for more details. Moreover, the splittings of the Stark sublevels reported in those studies are also between several tens and a few hundred centimeters^{-1}, similar to those calculated by us.[6d–f,23]

Scheme 1. Energy Diagram for the Substates of the Ground Multiplet of [(ZnL)Dy(hfac)$_2$] (**2·Dy**)

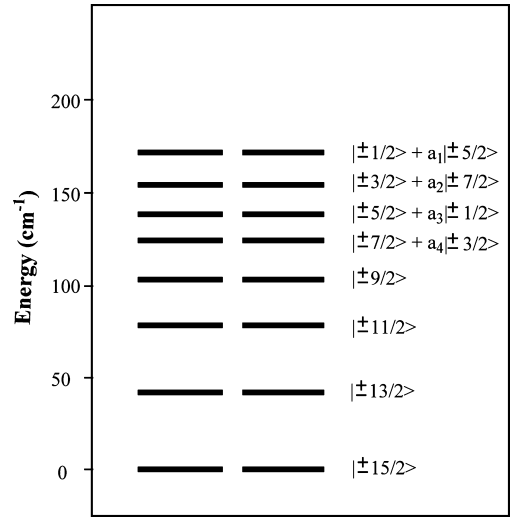

(18) Abragam, A.; Bleaney, B. *Electron Paramagnetic Resonance of Transition Ions*; Dover: New York, 1986.
(19) Casey, A. T.; Mitra, S. In *Theory and Applications of Molecular Paramagnetism*; Boudreaux, E. A., Mulay, L. N., Eds.; John Wiley & Sons: New York, 1976; pp 271−316.
(20) Benelli, C.; Caneschi, A.; Gatteschi, D.; Guillou, O.; Pardi, L. *Inorg. Chem.* **1990**, *29*, 1750–1755.
(21) Kahn, M. L.; Ballou, R.; Porcher, P.; Kahn, O.; Sutter, J.-P. *Chem.—Eur. J.* **2002**, *8*, 525–531.
(22) Tang, J.; Hewitt, I.; Madhu, N. T.; Chastanet, G.; Wernsdorfer, W.; Anson, C. E.; Benelli, C.; Sessoli, R.; Powell, A. K. *Angew. Chem., Int. Ed.* **2006**, *45*, 1729–1733.
(23) Przychodzen, P.; Pelka, R.; Lewinski, K; Supel, J.; Rams, M.; Tomala, K.; Sieklucka, B. *Inorg. Chem.* **2007**, *46*, 8924–8938.

The above results for the fitting of the $\chi_M T$ versus T curve for **2·Dy** are qualitatively confirmed by the analysis of the dependence of the reduced magnetization ($M/N\beta$) on the ratio H/T for several fields in the range 1−5 T (Figure S6, Supporting Information), performed with the same Hamiltonian, for which good fits could be obtained with the same g and D values (1.25 and −2.0 cm^{-1}, respectively), and similar values of E. Actually, the magnetization versus H/T curves in the range 2−5 K depends more markedly than the $\chi_M T$ versus T curves fitted in the range 2−50 K on the subtle splitting of the lowest levels determined by neglecting higher-order terms in the crystal field contribution, so that we could not find a unique value of E giving an accurate fit for all of the curves at different fields, but rather values spread around −0.7 cm^{-1}, in the range −0.5 to −2.0 cm^{-1}.

To obtain a quantitative estimate of the exchange coupling between the Dy^{III} and Ni^{II} ions, we used an approximate approach based on the assumption that the coupling energy between the dysprosium free ion ground state and the nickel ground spin state is much smaller than the interelectronic repulsion and the spin−orbit interaction. This avoids facing the most rigorous but complicated approach to the treatment of the exchange interactions, involving one orbitally degenerate lanthanide ion and one orbitally nondegenerate transition metal ion, based on the irreducible tensor operators.[24] With this approximation, we calculated the states for the dinuclear complex as a linear combination of the $^6H_{15/2}$ and the $S = 1$ spin states and thus described the exchange interaction between the Dy^{III} and Ni^{II} ions in **1·Dy**, using the following spin Hamiltonian based on an isotropic Heisenberg interaction term:

$$\mathbf{H} = g\beta(\mathbf{J}_{Dy} + \mathbf{S}_{Ni})H + D_{Dy}[\mathbf{J}^2_{Dyz} - J(J+1)/3] + E_{Dy}(\mathbf{J}^2_{Dyx} - \mathbf{J}^2_{Dyy}) + D_{Ni}[\mathbf{S}^2_{Niz} - S(S+1)/3] + 2J\mathbf{J}_{Dy}\mathbf{S}_{Ni} \quad (3)$$

where J is the coupling constant between the Dy^{III} and Ni^{II} ions and the other terms have their usual meaning. Such an isotropic treatment of the exchange interactions involving orbitally degenerate and nondegenerate spin centers has been recently applied to polynuclear lanthanide-transition metal or lanthanide-radical complexes.[21,23,25,26] Moreover, we assumed that the ligand field around Dy is the same in both **1·Dy** and **2·Dy** and used the same parameters D_{Dy} and E_{Dy} fitted for the isolated lanthanide ion in **2·Dy** in the spin Hamiltonian for **1·Dy** ($D = -2.0$ cm^{-1} and $E = -0.7$ cm^{-1}). Indeed, under the above assumption, also the energy spectrum of the Stark sublevels for the Dy^{III} ion should coincide, consistently with the same temperature dependence for these two complexes in the temperature range above 20 K. Also for the ZFS parameter of Ni, D_{Ni}, we used the same value fitted from the isostructural complex **1·Gd** ($D = +1.5$ cm^{-1}). We performed a fitting with the above Hamiltonian considering only the susceptibility values below 50 K, where the exchange interactions between Dy^{III} and Ni^{II} operate, to more accurately reproduce the J value. A good fit could be obtained ($R = 2.6 \times 10^{-5}$) with $g = 1.27$ and J(Dy−Ni) = 0.14 cm^{-1}, see the solid line in Figures 4 and 5, the small positive ferromagnetic exchange coupling constant being consistent with the small increase of $\chi_M T$ only below 10 K.

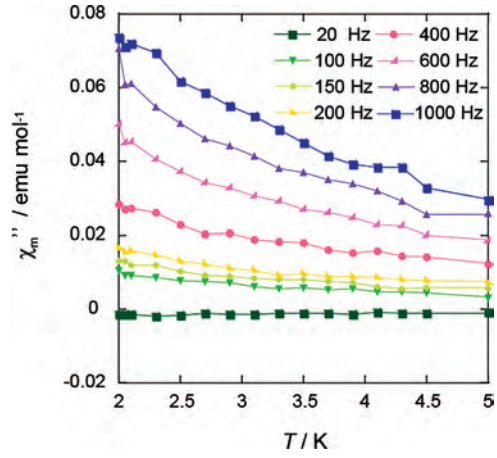

Figure 6. Plots of the out-of-phase (χ_M'') ac susceptibility signal vs temperature for the complex [(NiL)Dy(hfac)$_2$] (**1·Dy**).

The smaller energy splitting of the exchange coupling compared with that of the crystal field prevents an analysis of the dependence of the reduced magnetization ($M/N\beta$) of **1·Dy** on the ratio H/T in terms of an isolated ground state. However, the magnetization curves, reported in Figure S7 (Supporting Information) for several fields in the range 1−5 T, are consistent with the ferromagnetic exchange between $Dy^{III}$and Ni^{II}, showing a saturation at a value higher than that shown by **2·Dy**.

The temperature dependence of magnetic susceptibility of **2·Eu** (Figure S3, Supporting Information) can be reproduced by the expression that we reported previously.[27] A reasonable fit could be obtained for λ (spin−orbit coupling constant) = 382 cm^{-1}. The fitting was much improved including a small temperature-independent parameter (TIP), leading to $\lambda = +310$ cm^{-1} and TIP = 9×10^{-4}. The λ value is comparable with those for other Eu^{III} ions in an analogous coordination environment.

The experimental values of the $\chi_M T$ and saturation magnetization for **2·Dy** indicate that the ground state of the Dy ions in the ligand crystal field is given by the maximum values of $|J_z\rangle$, ±15/2, being separated from the first excited states by ca. 40 cm^{-1}, and thus that the single Dy ion has an Ising-type anisotropy. This, together with the observed ferromagnetic Dy−Ni interaction and the high value of $\chi_M T$, suggests that **1·Dy** is a good candidate for a SMM. One of the characteristics of a SMM is the observation of an out-of-phase (χ_M'') ac susceptibility signal. The ac susceptibility measurements were carried out in a 3.0 G ac field oscillating at 20−1000 Hz in the temperature range of 2.0−5.0 K, and with a zero dc magnetic field (Figure 6). The out-of-phase susceptibility (χ_M'') begins to increase at ca. 5 K at all tested frequencies; this trend continues as the temperature is decreased. In addition, the out-of-phase susceptibility is frequency-dependent. However, the

(24) Levy, P. M. *Phys. Rev.* **1964**, *135*, A155−165.
(25) Trojan, K. L.; Kendall, J. L.; Kepler, K. D.; Hatfield, W. E. *Inorg. Chim. Acta* **1992**, *198*−*200*, 795–803.
(26) Sanz, J. L.; Ruiz, R.; Gleizes, A.; Lloret, F.; Faus, J.; Julve, M.; Borràs-Almenar, J. J.; Journausx, Y. *Inorg. Chem.* **1996**, *35*, 7384–7393.
(27) Kido, T.; Ikuta, Y.; Sunatsuki, Y.; Ogawa, Y.; Matsumoto, N.; Re, N. *Inorg. Chem.* **2003**, *42*, 398–408.

χ_M'' signal is quite weak: at its maximum at the lowest accessible temperature of 2 K, it is only 1−2% of the in-phase χ_M' signal. Moreover, because of the 2 K temperature limit of the instrument, a maximum in χ_M'' was not observed at frequencies as high as 1000 Hz. As a result of the low blocking temperature (T_B < 2 K), we did not observe hysteresis behavior in the magnetization of this sample. Plots of the in-phase (χ_M') ac susceptibility signal versus temperature did not show frequency dependence. We then considered the two lanthanide analogs (Ln = Gd, Tb) of **1·Dy**, **1·Gd**, and **1·Tb**, whose crystal structures have been shown to be isostructural (see above). Neither of them exhibits an out-of-phase component in the ac experiment, even though they retain high χT values at low temperatures.

Conclusions

By using $[NiL]^-$ as the *ligand complex*, heterodinuclear [(NiL)Ln(hfac)$_2$(EtOH)] (**1·Ln**; Ln = Eu, Gd, Tb, and Dy) complexes were prepared. A ferromagnetic interaction between Ni^{II} and Ln^{III} was indicated in **1·Gd**, **1·Tb**, and **1·Dy**. The magnetic interaction between Ni^{II} and Eu^{III} is negligible in **1·Eu**. **1·Dy** is the first dinuclear Ni^{II}−Dy^{III} complex to display the frequency dependence of the out-of-phase component (χ_M'') characteristic of SMMs, although the weakness of the χ_M'' signal and absence of a maximum in the χ_M'' versus T curve make the SMM nature of **1·Dy** questionable. The low blocking temperature (T_B < 2 K) of **1·Dy** seems to be related to the chain structure resulting from $\pi-\pi$ stacking between the neighboring molecules. We have not observed magnetization hysteresis, the diagnostic property of a magnet. Efforts are currently underway to eliminate intermolecular interactions by introducing bulky substituents on the ligand. The present study demonstrates that the synthesis of 3d−4f complexes is a promising approach to SMMs. We can easily prepare dinuclear $Ni^{II}Ln^{III}$, trinuclear $Ni^{II}Ln^{III}Ni^{II}$, and tetranuclear $Ni^{II}Ln^{III}Ln^{III}Ni^{II}$ complexes by the use of the "complexes-as-ligands" strategy, and the nuclearity of the complexes can be controlled by the selection of the additional ligand on the Ln^{III} ion. We expect that the trinuclear and tetranuclear 3d−4f complexes will easily satisfy the conditions for SMMs with a high-spin ground state and a magnetic anisotropy, and studies along this line are in progress in our laboratories.

Experimental Section

Materials. All reagents and solvents in the syntheses were of reagent grade, and they were used without further purification. The H_3L ligand,[7] $[Ni(H_{1.5}L)]Cl_{0.5}\cdot MeOH$ (**1**),[10] $[Zn(H_{1.5}L)](ClO_4)_{0.5}\cdot 1.5MeOH$ (**2**),[10] and $[Ln(hfac)_3(H_2O)_2]$ (Ln = Eu, Gd, Tb, Dy)[28] were prepared according to the literature procedure.

[(NiL)Ln(hfac)$_2$(EtOH)] (Ln = Eu (1·Eu), Gd (1·Gd), Tb (1·Tb), and Dy (1·Dy)). All of these complexes were prepared by a similar method. A representative procedure is given for **1·Eu**. $[Eu(hfac)_3(H_2O)_2]$ (0.163 g, 0.2 mmol) in ethanol (20 mL) and Et_3N (0.02 g, 0.2 mmol) in ethanol (10 mL) were added to an ethanol solution (20 mL) of $[Ni(H_{1.5}L)]Cl_{0.5}$ (0.097 g, 0.2 mmol). The mixture was left at room temperature to deposit pale yellow crystals. They were collected by filtration and dried *in vacuo*. The coordinated ethanol was lost upon drying. Yield: 0.119 g (60%). Anal. Calcd for $C_{36}H_{26}F_{12}EuN_3O_7Ni$, [(NiL)Eu(hfac)$_2$]: C; 41.13, H; 2.49, N; 3.99%. Found: C; 40.86, H; 2.21, N; 3.83%. IR (KBr disk): ν (C=N) 1635; ν(C=O) 1652, 1664; ν(C−F) 1143, 1198, 1254 cm^{-1}.

1·Gd. Dichroic (pale green and pink) crystals. Yield: 54%. Anal. Calcd for $C_{36}H_{26}F_{12}GdN_3O_7Ni$, [(NiL)Gd(hfac)$_2$]: C; 40.92, H; 2.48, N; 3.98%. Found: C; 41.10, H; 2.52, N; 3.80%. IR (KBr disk): ν(C=N) 1634; ν(C=O) 1652, 1664; ν(C−F) 1143, 1198, 1254 cm^{-1}.

1·Tb. Dichroic (pale green and pink) crystals. Yield: 69%. Anal. Calcd for $C_{36}H_{26}F_{12}TbN_3O_7Ni$, [(NiL)Tb(hfac)$_2$]: C; 40.86, H; 2.47, N; 3.97%. Found: C; 40.96, H; 2.23, N; 3.82%. IR (KBr disk): ν(C=N) 1634; ν(C=O) 1648, 1662; ν(C−F) 1143, 1211, 1255 cm^{-1}.

1·Dy. Dichroic (pale green and pink) crystals. Yield: 70%. Anal. Calcd for $C_{36}H_{26}F_{12}DyN_3O_7Ni$, [(NiL)Dy(hfac)$_2$]: C; 40.72, H; 2.47, N; 3.95%. Found: C; 40.89, H; 2.22, N; 3.65%. IR (KBr disk): ν(C=N) 1634; ν(C=O) 1648, 1663; ν(C−F) 1141, 1213, 1255 cm^{-1}.

[(ZnL)Ln(hfac)$_2$(EtOH)] (Ln = Eu (2·Eu), Gd (2·Gd), Tb (2·Tb), and Dy (2·Dy)). These complexes were prepared by a similar method, and a representative procedure is given for **2·Gd**. An ethanol suspension (20 mL) of $[Gd(hfac)_3(H_2O)_2]$ (0.32 g, 0.40 mmol) was added to an ethanol solution (50 mL) of $[Zn(H_{1.5}L)](ClO_4)_{0.5}$ (0.22 g, 0.40 mmol). Triethylamine (0.12 g, 1.2 mmol) in ethanol (20 mL) was added to the mixture. The solution was left at room temperature for several days to form pale yellow plates. They were collected by filtration. The coordinated ethanol was lost upon drying. Yield: 0.045 g (11%). Anal. Calcd for $C_{36}H_{26}F_{12}GdN_3O_7Zn$, [(ZnL)Gd(hfac)$_2$]: C; 40.66, H; 2.46, N; 3.95%. Found: C; 40.74, H; 2.00, N; 3.90%. IR (KBr disk): ν(C=N) 1635; ν(C=O) 1648, 1662; ν(C−F) 1143, 1210, 1254 cm^{-1}.

2·Eu. Pale yellow crystals. Yield: 14%. Anal. Calcd for $C_{36}H_{26}F_{12}EuN_3O_7Zn$, [(ZnL)Eu(hfac)$_2$]: C; 40.87, H; 2.47, N; 3.97%. Found: C; 40.80, H; 2.29, N; 3.86%. IR (KBr disk): ν(C=N) 1635; ν(C=O) 1650, 1664; ν(C−F) 1143, 1198, 1253 cm^{-1}.

2·Tb. Pale yellow plates. Yield: 14%. Anal. Calcd for $C_{36}H_{26}F_{12}TbN_3O_7Zn$, [(ZnL)Tb(hfac)$_2$]: C; 40.60, H; 2.46, N; 3.94%. Found: C; 40.98, H; 1.95, N; 3.98%. IR (KBr disk): ν(C=N) 1636; ν(C=O) 1650, 1665; ν(C−F) 1143, 1199, 1254 cm^{-1}.

2·Dy. Pale yellow crystals. Yield: 6%. Anal. Calcd for $C_{36}H_{26}F_{12}DyN_3O_7Zn$, [(ZnL)Dy(hfac)$_2$]: C; 40.46, H; 2.45, N; 3.93%. Found: C; 40.56, H; 1.88, N; 3.90%. IR (KBr disk): ν(C=N) 1634; ν(C=O) 1648, 1664; ν(C−F) 1146, 1211, 1255 cm^{-1}.

Physical Measurements. Elemental analyses (C, H, N) were performed on a Perkin-Elmer 2400II elemental analyzer. IR spectra were recorded on a JASCO FT/IR FT-550 spectrophotometer with the samples prepared as KBr disks. Magnetic susceptibility measurements of thoroughly ground samples were carried out on a Quantum Design MPMS XL5 SQUID magnetometer at Okayama University of Science in the temperature range 1.9−300 K and under an applied magnetic field of 0.1 T. Magnetization versus magnetic field measurements were carried out at 1.9 K in the field range 0−5 T. For magnetic measurements, samples were placed into a gelatin capsule, which was placed inside a plastic straw. Corrections for diamagnetism were applied by the use of Pascal's constants. Alternating-current magnetic measurements were carried out at the University of Wrocław in a 3.0 G ac field oscillating at 20−1000 Hz in the temperature range of 2.0–5.0 K.

X-ray Data Collection, Reduction, and Structure Determination. A suitable crystal obtained from an ethanol or a methanol solution was placed in a capillary tube with a small amount of mother liquid. The X-ray measurements were made on a Rigaku RAXIS

(28) Richardson, M. F.; Wagner, W. F.; Sands, D. E. *J. Inorg. Nucl. Chem.* **1968**, *30*, 1275–1289.

RAPID II (Okayama University) or a Rigaku RAXIS-IV (Okayama University of Science) imaging plate area detector with graphite monochromated Mo Kα radiation ($\lambda = 0.710\,69$ Å). The structures were determined by direct methods (*SHELXS97* or *SIR97*[29]) and expanded using Fourier techniques[30] and successive Fourier difference methods with full-matrix least-squares refinement on F^2. The non-hydrogen atoms were refined anisotropically. Hydrogen atoms were refined using the riding model. All calculations were performed using the *Crystal Structure 3.8* software package.[31]

Calculations of Magnetic Properties. Magnetization and magnetic susceptibility at each temperature were calculated using the following theoretical equation:[14]

$$M = \left[N\sum\nolimits_i (-\mathrm{d}E_i/\mathrm{d}H)\exp(-E_i/kT)\right]/\left[\sum\nolimits_i \exp(-E_i/kT)\right]$$

$$\chi = M/H$$

The energy levels, E_i, of the considered systems were evaluated by diagonalizing the Hamiltonian matrix built from the corresponding operator in the uncoupled spin function basis set (with dimensions 16 × 16 for **2·Dy** and 48 × 48 for **1·Dy**).

We wrote a program, including ZFS and the rhombic distortion of the single ions (E), to calculate χ_M and M for two coupled ions of any S according to the above equation.

Acknowledgment. This work was supported in part by a Grant-in-Aid for Scientific Research (Nos. 16205010, 16750050, and 17350028) from the Ministry of Education, Culture, Sports, Science and Technology of Japan; by the Iketani Science and Technology Foundation; and also by the EU 6FP MAGMANet Programme. T.Y. was supported by the JSPS program for Research Fellowships for Young Scientists (No. 17003601).

Supporting Information Available: X-ray crystallographic files in CIF format for compounds H_3L, **1·Eu**, **1·Gd**, **1·Tb**, **1·Dy**, **2·Eu**, **2·Gd**, **2·Tb**, and **2·Dy**; ORTEP drawing of **2·Gd** (Figure S1); field dependence of magnetization for **1·Gd** (Figure S2); magnetic behavior of **2·Ln** (Figure S3); plots of $\chi_M T$ vs T for **1·Tb** and **2·Tb**; the difference $\Delta(T)$ (Figure S4) and plots of $\chi_M T$ vs T for **1·Eu** and **2·Eu**; the difference $\Delta(T)$ (Figure S5) and reduced magnetization vs H/T for **2·Dy** (Figure S6); reduced magnetization vs H/T for **1·Dy** (Figure S7); and Appendix A. This material is available free of charge via the Internet at http://pubs.acs.org.

IC8000575

(29) (a) Sheldrick, G. M. *SHELXS97*; University of Göttingen: Göttingen, Germany, 1997. (b) Altomare, A.; Burla, M.; Moliterni, A.; Polidori, G.; Spagna, R. *J. Appl. Crystallogr.* **1999**, *32*, 115–119.

(30) Beurskens, P. T.; Admiraal, G.; Beurskens, G.; Bosman, W. P.; de Gelder, R.; Israel, R.; Smits, J. M. M. *DIRDIF99: The DIRDIF-99 program system*, Technical Report of the Crystallography Laboratory, University of Nijmegen, The Netherlands, 1999.

(31) *CrystalStructure 3.8, Crystal Structure Analysis Package*; Rigaku and Rigaku/ MSC: The Woodlands, TX, 2001−2006.